Vibration Analysis on A Three-support Rotor System with Star Gear Transmission Components

Dongjie Chen, Hao Zhang, Jinyu Zhai, Qingkai Han*

School of Mechanical Engineering, Dalian University of Technology, Dalian, China PR

Abstract: Considering the dynamic characteristics of the low pressure rotors in a geared turbofan (GTF) aero-engine, a model of three-support rotor system with star-geared transmission components is proposed. Taking the coupling between fan rotor and low pressure compressor-turbine rotor, the dynamic model is built by finite element method. Then, comparing the calculations of modes of its first orders with the results of simulations analysis and experiments, and the validity of the modeling approach is verified. The differences are clarified by modal analyses on the single rotor and the combined one. From the results, the fan rotor and low pressure compressor-turbine rotor separately causes deviation of natural frequencies and loss of special modes. Based on the combined model of the GTF low pressure rotor system, the vibration behaviors are studied under three rotational speed and different imbalance conditions. From the results of theoretical and experimental analysis, the imbalance of the low pressure compressor-turbine rotor has a greater impact on the vibration characteristics of the gearbox than the fan rotor. From the frequency spectra of imbalance responses, not only rotating frequency but also multiple frequencies appear due to the coupling statements of the rotor system herein, and the ratio of multiple frequencies changes with rotational speed certainly.

Keywords: Geared turbo fan engine (GTF); star-geared components; Three-support rotor system; Coupling vibration; imbalances vibration

1 Introduction

With the development of science and technology, in order to further improve fuel economy and reduce pollutant emissions, future commercial aero-engines will technically focus on designing low pressure rotors and fan rotors to work at optimal speeds. For this technology, PW developed a Geared Turbofan(GTF) [1] which introduces a star gear transmission system between the fan and the low pressure compressor-turbine rotor to reduce the fan speed, which will reduce fuel consumption and noise [2]. Because of the existence of the gearbox, the vibration characteristics of the rotor system are greatly different from the traditional aero-engine rotor model. Moreover, the high rotation speed makes the slender low pressure rotor a flexible rotor,

* Corresponding author: Qingkai Han (hanqingkai@dult.edu.cn)

and there may be multi-stage resonant speed at the working speed. Therefore, the dynamic characteristics of the GTF rotor system has gradually become a hot topic.

GTF low pressure rotor system, a three-support rotor with star gear transmission system, poses new challenges to the structural and dynamic design of rotor systems. Recent years, some domestic scholars have studied the dynamic characteristics of the star-gear transmission system [3-5], but mostly stay in the gear dynamics. Few researches have been done on the rotor dynamic characteristics.

In the related research on the GTF rotor system, in addition to the general analysis of the structure and technical characteristics, some scholars [6-7] have also performed a series of analysis on the dynamic characteristics of the low-pressure rotor system. However, most of the studies have extracted the low-pressure rotor separately or greatly simplified the coupling of the gears. For the vibration problem of such systems, if the influence of coupled vibration is not considered comprehensively, not only is the calculation accuracy low, but also will the result ignore some important dynamic characteristics, making it difficult to provide a comprehensive basis for shafting vibration analysis.

Taking the low pressure rotor system of GTF as the object, the author has established a three-support rotor with star gear transmission system following the structural similarity to model the rotor system. Based on the finite element method, a finite element dynamic model with a few degrees of freedom for the rotor system is established. With the dynamic solver program of MATLAB, Newmark stepwise integration method [8] is used to calculate the inherent characteristics of the low pressure rotor system. Sambef Field is used to establish the simulation model, which verifies the correctness of the modeling method. The influence of gear coupling on the dynamic characteristics of the rotor system is analyzed. Furthermore, different working conditions are set to study the unbalanced response of the rotor system, which lead to a foundation for further study on the vibration transmission law of the low pressure rotor system of the GTF.

2 The dynamic model of low pressure rotor system

2.1 Characteristics of GTF low pressure rotor system

The GTF low pressure rotor system consists of a fan assembly, a low pressure turbine assembly, a low pressure compressor assembly, and a gear transmission assembly, as shown in Figure 1. Fan rotor, gearbox and low pressure compressor- turbine rotor are supported individually. The fan rotor is cantilevered over two side-by-side tapered roller bearings (Support 1 in Figure 1). The low pressure rotor adopts a two-support structure, which is a 0-1-1 support scheme, with two supports located near the low-pressure compressor and the center of the low-pressure turbine (Support 2, 3 in Figure 1) and are respectively supported by ball bearings and stick bearings. The rear shaft of the low pressure compressor is connected to the low pressure turbine shaft through a transitional short shaft [9]. The rotor shaft is slender. The compressor and turbine disks are relatively large. The gearbox is a star-gear transmission with a transmission ratio of approximately 3:1 [10-11]. The ring gear serves as the output end and is connected with

 ISSN 2572-4975 (Print), 2572-4991 (Online)

the fan rotor; the sun gear serves as the input end and is connected with the low pressure compressor-turbine rotor; the output shaft is rotating in counter direction of the input shaft.

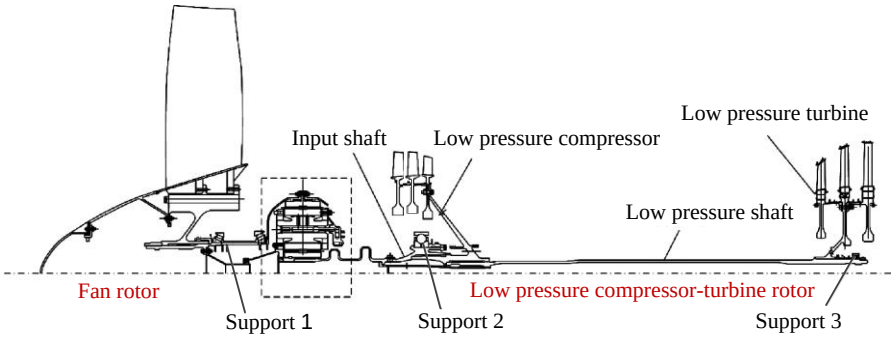

Fig. 1. Structure of GTF low pressure rotor system

2.2 The three-support rotor with star gear transmission system modeling

For the low pressure rotor system of PW1000G geared turbofan engine, the influence of the gear connection and the supporting structure of the system on the dynamic characteristics of the rotor system is studied. According to the structural similarity of the complex rotating power equipment and the design principle of equal-proportion model, the rotor system is modeled, and a three-support rotor with star gear transmission system is established.

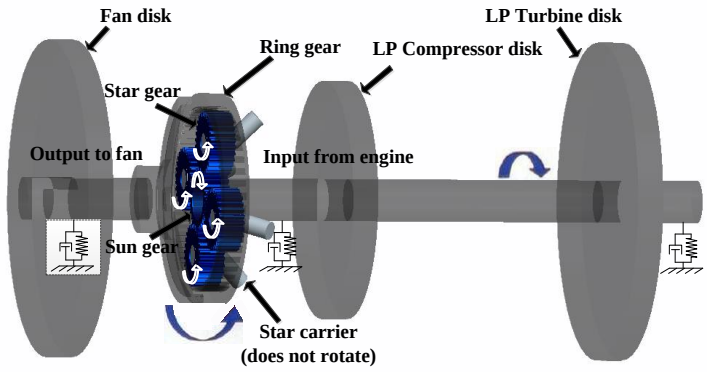

(a) Schematic diagram

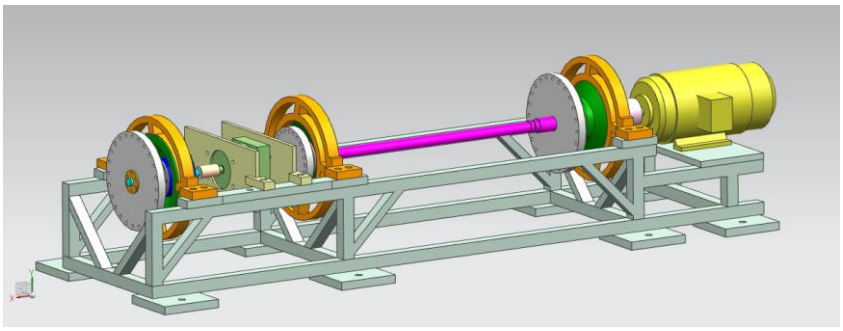

(b) Outline drawing

Fig. 2. Structure of GTF engine low pressure rotor experiment rig

As shown in Figure 2, the rotor system is mainly composed of a fan rotor, a low pressure compressor-turbine rotor, and a gearbox. The fan rotor is cantilevered over an elastic support, and its right-end is connected to the reducer's output shaft through a coupling; the low pressure compressor-turbine rotor adopts the 0-1-1 two-support method and its left-end is connected to reducer's input shaft. The bearings used for the three supports of the rotor are the same as the prototypes, in sequences are two paratactic tapered roller bearings, a deep groove ball bearing and a cylindrical roller bearing. According to the mass distribution's characteristics of the fan and the low-pressure compressor-turbine rotor of the prototype, turntables are set in the corresponding positions.

The star gear transmission in the low-pressure rotor system is composed of a sun gear, four planetary gears and a ring gear. It is independent supported by a plate, and the transmission ratio is 3:1. The gear parameters are shown in Table 1.

Table 1. Gear parameters

Part name	Number of teeth	Modu-lus	Pressure an-gle	Face width
Sun gear	30	0.8	20	10
Planetary gear	30	0.8	20	10
Ring gear	90	0.8	20	10

The finite element model of the rotor system is established. The shaft section is modeled with beam elements. The disc and gears adopt the lumped mass model. The coupling effect of the gear is realized via the stiffness assembly [12-15]. The mechanical model of the transmission part of the system is shown in Figure 3. The specific modeling process is as follows.

ISSN 2572-4975 (Print), 2572-4991 (Online)

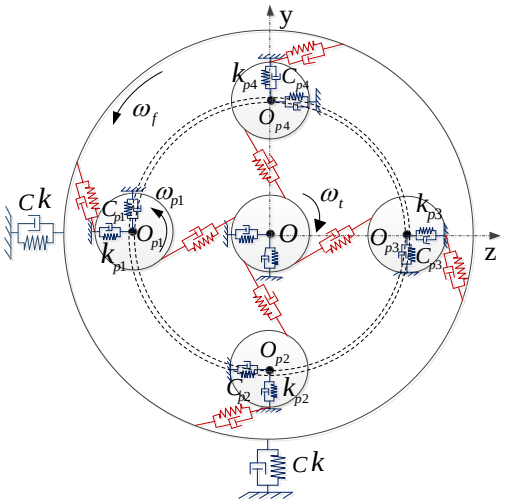

Fig. 3. The mechanical model of the star gear transmission

(1) Gear engagement unit

The effect of the complex star gear transmission on the rotor is considered as the spring stiffness. The meshing stiffness is brought into the meshing part of the eight pairs of gear teeth to establish stiffness units.

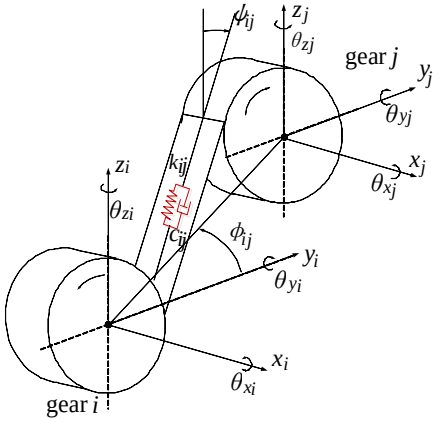

Fig. 4. The Dynamic model of meshing part

In Figure 4, *i* and *j* are a pair of spur gears meshing with each other, where *i* is the driving wheel and *j* is the driven wheel. Each gear has three degrees of translational freedom and three degrees of rotational freedom. The element has a total of 12 degrees of freedom. $\boldsymbol{u}$ is the displacement vector of the pair of gears and it is expressed as

$$\boldsymbol{u}=[x_i,y_i,z_i,\theta_{xi},\theta_{yi},\theta_{zi},x_j,y_j,z_j,\theta_{xj},\theta_{yj},\theta_{zj}]^{\mathrm{T}}$$

In the dynamic model of the meshing of the star gear, Ψ_{ij} is the direction angle from the positive direction of the z-axis to the meshing surface. It is related to the direction of rotation of the driving wheel and is expressed as

$$\psi_{ij} = \begin{cases} \alpha_{ij} - \phi_{ij} & \textit{driven in counter} - \textit{clockwise direction} \\ -\alpha_{ij} - \phi_{ij} & \textit{driven in clockwise direction} \end{cases}$$

Where α_{ij} is the pressure angle of the gear and ϕ_{ij} is the angle between the center line of the gear and the positive direction of the y-axis.

The equation of motion of the gear pairs is

$$\begin{aligned} & m_i \ddot{y}_i + [c_{ij}\dot{p}_{ij}(t) + k_{ij}p_{ij}(t)]\sin\psi_{ij} = 0 \\ & m_i \ddot{z}_i + [c_{ij}\dot{p}_{ij}(t) + k_{ij}p_{ij}(t)]\cos\psi_{ij} = 0 \\ & I_{pi}\ddot{\theta}_{xi} + \operatorname{sgn} r_i[c_{ij}\dot{p}_{ij}(t) + k_{ij}p_{ij}(t)] = T_i \\ & m_j \ddot{y}_j - [c_{ij}\dot{p}_{ij}(t) + k_{ij}p_{ij}(t)]\sin\psi_{ij} = 0 \\ & m_j \ddot{z}_j - [c_{ij}\dot{p}_{ij}(t) + k_{ij}p_{ij}(t)]\cos\psi_{ij} = 0 \\ & I_{pj}\ddot{\theta}_{xj} - \operatorname{sgn} r_j[c_{ij}\dot{p}_{ij}(t) + k_{ij}p_{ij}(t)] = -T_j \\ & m_i \ddot{x}_i = m_j \ddot{x}_j = 0 \\ & I_{dj}\ddot{\theta}_{yj} = I_{di}\ddot{\theta}_{zi} = 0 \\ & I_{dj}\ddot{\theta}_{zj} = I_{di}\ddot{\theta}_{zi} = 0 \end{aligned} \tag{1}$$

Where T_i is the driving torque, k_{ij} is the meshing stiffness, c_{ij} is the meshing damping, $p_{ij}(t)$ is the relative displacement of the teeth along the meshing line. $p_{ij}(t)$ is mainly composed of the torsional deformation p_{ijr} and the vibratory deformation p_{ijl} , which is obtained as

$$\begin{aligned} & p_{ij}(t) = p_{ijr} + p_{ijl} \\ & = sgnr_i\theta_{xi} + sgnr_j\theta_{xj} + (y_i - y_j)\sin\psi_{ij} + (z_i - z_j)\cos\psi_{ij} \end{aligned}$$

Where r_i and r_j are the base radius of gears i and j, respectively. sgn is a sign function and is defined by:

$$sgn = \begin{cases} 1 & \textit{driven in counter} - \textit{clockwise direction} \\ -1 & \textit{driven in clockwise direction} \end{cases}$$

For the gear meshing unit, the equation (1) is converted into the matrix as

$$\boldsymbol{M}_{ij}\ddot{\boldsymbol{u}} + \boldsymbol{C}_{ij}\dot{\boldsymbol{u}} + \boldsymbol{K}_{ij}\boldsymbol{u} = \boldsymbol{F} \tag{2}$$

In equation (2), $\boldsymbol{F}$ is the generalized force vector of the gear unit. $\boldsymbol{M_{ij}}$, $\boldsymbol{C_{ij}}$, and $\boldsymbol{K_{ij}}$ are the mass matrix, damping matrix, and meshing stiffness matrix of the gear unit, respectively, written as:

ISSN 2572-4975 (Print), 2572-4991 (Online)

$$\boldsymbol{M}_{ij}=\begin{pmatrix} m_i & & & & & & & & & & & \\ & m_i & & & & & & & & & & \\ & & m_i & & & & & & & & & \\ & & & J_i & & & & & & & & \\ & & & & I_i & & & & & & & \\ & & & & & I_i & & & & & & \\ & & & & & & m_j & & & & & \\ & & & & & & & m_j & & & & \\ & & & & & & & & m_j & & & \\ & & & & & & & & & J_j & & \\ & & & & & & & & & & I_j & \\ & & & & & & & & & & & I_j \end{pmatrix}$$

$$\boldsymbol{C}_{ij}=c_{ij}\cdot\boldsymbol{a}_{ij}^{\mathrm{T}}\cdot\boldsymbol{a}_{ij}=\begin{pmatrix} c_{1,1} & \cdots & c_{1,12} \\ \vdots & \ddots & \vdots \\ c_{12,1} & \cdots & c_{12,12} \end{pmatrix} \qquad \boldsymbol{K}_{ij}=k_{ij}\cdot\boldsymbol{a}_{ij}^{\mathrm{T}}\cdot\boldsymbol{a}_{ij}=\begin{pmatrix} k_{1,1} & \cdots & k_{1,12} \\ \vdots & \ddots & \vdots \\ k_{12,1} & \cdots & k_{12,12} \end{pmatrix}$$

Where

$$\boldsymbol{a}_{ij}=[0 \quad \sin\psi_{ij} \quad \cos\psi_{ij} \quad \operatorname{sgn} r_i \quad 0 \quad 0$$
$$0 \quad -\sin\psi_{ij} \quad -\cos\psi_{ij} \quad \operatorname{sgn} r_j \quad 0 \quad 0]$$

Since the meshing stiffness will change with the rotation of the gears in actual meshing, the time-varying property of the meshing stiffness is considered for k_{ij}, which is related to the contact ratio and the stiffness of the teeth. Take the pair of meshed sun and planet gears in this study as an example. The driving wheel's speed is set as 9000 r/min. According to the of Ishikawa formula [16-17], the meshing stiffness curve of the pair of gears can be obtained, as shown in the Figure 5.

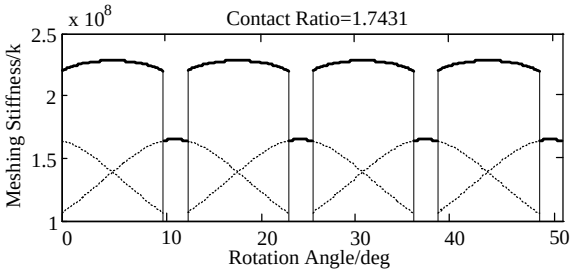

Fig. 5. The curve of the meshing stiffness of gears

The contact ratio of the pair of gears is greater than 1, and the stiffness curve has a significant jump phenomenon. In the double-meshing area, there are two pairs of gear teeth engaged at the same time. The stiffness is the superposition of the stiffness of the two pairs of gear teeth. The meshing area is long and the average stiffness is large.

The time-varying meshing stiffness is considered. The Fourier series is used to fit one cycle of stiffness curve. The time-varying meshing stiffness can be expressed as:

$$k_{ij} = a_0 + \sum_{i=1}^{n} \left(a_i \cos(i\omega t) + b_i \sin(i\omega t) \right)$$

(2) Shaft section unit

By finite element method, the shaft is simplified as a flexible shaft sections and nodes with concentrated mass. The shaft section unit is the space beam element. As shown in Figure 6, the beam element has two nodes *A* and *B*. Each node has 6 degrees of freedom. The generalized coordinates of the elements are:

$$\boldsymbol{u}^{e} = \left[x_A \quad y_A \quad z_A \quad \theta_{xA} \quad \theta_{yA} \quad \theta_{zA} \quad x_B \quad y_B \quad z_B \quad \theta_{xB} \quad \theta_{yB} \quad \theta_{zB} \right]^{\mathrm{T}}$$

Where *A* and *B* represent the two nodes of the beam element. *x*, *y*, *z* are the line displacements of the corresponding nodes in the three directions in the local coordinate system. θ_x, θ_y, θ_z are the rotations of the cross sections of the corresponding nodes around the three coordinate axes.

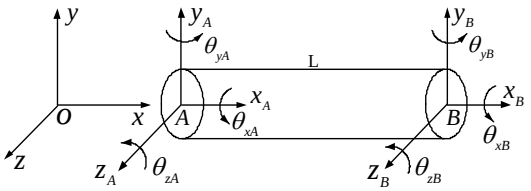

Fig. 6. The schematic diagram of shaft section unit

Based on the fixed coordinate system *O-XYZ*, the differential equation of motion of the beam element is:

$$\boldsymbol{M}^{e}\ddot{\boldsymbol{u}}^{e} + \Omega \boldsymbol{G}^{e}\dot{\boldsymbol{u}}^{e} + \boldsymbol{K}^{e}\boldsymbol{u}^{e} = \boldsymbol{F}^{e} \tag{3}$$

In equation (3), Ω is the rotational speed of the beam element around the *x* axis, $\boldsymbol{F}^{e}$ is the generalized force vector on the beam element. $\boldsymbol{M}^{e}$, $\boldsymbol{G}^{e}$ and $\boldsymbol{K}^{e}$ are the mass matrix, the gyro force matrix and the stiffness matrix of the beam element, respectively, which can be expressed in the following forms.

$$\boldsymbol{M}^{e} = \rho AL \begin{bmatrix}
1/3 & & & & & & & & & & & \\
0 & M_a & & & & & & & & & & \\
0 & 0 & M_a & & & & & & & & & \\
0 & 0 & 0 & JA/3 & & & & & & & & \\
0 & 0 & -M_c & 0 & M_e & & & & & & & \\
0 & M_c & 0 & 0 & 0 & M_e & & & & & & \\
1/6 & 0 & 0 & 0 & 0 & 0 & 1/3 & & & & & \\
0 & M_b & 0 & 0 & 0 & M_d & 0 & M_a & & & & \\
0 & 0 & M_b & 0 & -M_d & 0 & 0 & 0 & M_a & & & \\
0 & 0 & 0 & JA/6 & 0 & 0 & 0 & 0 & 0 & JA/3 & & \\
0 & 0 & M_d & 0 & M_f & 0 & 0 & 0 & M_c & 0 & M_e & \\
0 & -M_d & 0 & 0 & 0 & M_f & 0 & -M_c & 0 & 0 & 0 & M_e
\end{bmatrix}$$

symmetry

Where

ISSN 2572-4975 (Print), 2572-4991 (Online)

$$M_a=\frac{\frac{13}{35}+\frac{7}{10}\phi^s+\frac{1}{3}(\phi^s)^2+\frac{6}{5}(r/L)^2}{(1+\phi^s)^2},\quad M_b=\frac{\frac{9}{70}+\frac{3}{10}\phi^s+\frac{1}{6}(\phi^s)^2-\frac{6}{5}(r/L)^2}{(1+\phi^s)^2},$$

$$M_c=\frac{\left(\frac{11}{210}+\frac{11}{120}\phi^s+\frac{1}{24}(\phi^s)^2+(\frac{1}{10}-\frac{1}{2}\phi^s)(r/L)^2\right)L}{(1+\phi^s)^2},\quad M_d=\frac{\left(\frac{13}{420}+\frac{3}{40}\phi^s+\frac{1}{24}(\phi^s)^2-(\frac{1}{10}-\frac{1}{2}\phi^s)(r/L)^2\right)L}{(1+\phi^s)^2},$$

$$M_e=\frac{\left(\frac{1}{105}+\frac{1}{60}\phi^s+\frac{1}{120}(\phi^s)^2+(\frac{2}{15}+\frac{1}{6}\phi^s+\frac{1}{3}(\phi^s)^2)(r/L)^2\right)L^2}{(1+\phi^s)^2},$$

$$M_f=\frac{\left(\frac{1}{140}+\frac{1}{60}\phi^s+\frac{1}{120}(\phi^s)^2+(\frac{1}{30}+\frac{1}{6}\phi^s-\frac{1}{6}(\phi^s)^2)(r/L)^2\right)L^2}{(1+\phi^s)^2}.$$

$$\boldsymbol{K}^e=\begin{bmatrix}
AE/L & & & & & & & & & & & \\
0 & K_a & & & & & & & & & & \\
0 & 0 & K_a & & & & & & \textit{symmetry} & & & \\
0 & 0 & 0 & GJ/L & & & & & & & & \\
0 & 0 & -K_b & 0 & K_c & & & & & & & \\
0 & K_b & 0 & 0 & 0 & K_c & & & & & & \\
-AE/L & 0 & 0 & 0 & 0 & 0 & AE/L & & & & & \\
0 & -K_a & 0 & 0 & 0 & -K_b & 0 & K_a & & & & \\
0 & 0 & -K_a & 0 & K_b & 0 & 0 & 0 & K_a & & & \\
0 & 0 & 0 & -GJ/L & 0 & 0 & 0 & 0 & 0 & GJ/L & & \\
0 & 0 & -K_b & 0 & K_d & 0 & 0 & 0 & K_b & 0 & K_c & \\
0 & K_b & 0 & 0 & 0 & K_d & 0 & -K_b & 0 & 0 & 0 & K_c
\end{bmatrix}$$

Where

$$K_a=\frac{12EI}{L^3\left(1+\phi^s\right)},\quad K_b=\frac{6EI}{L^2\left(1+\phi^s\right)},\quad K_c=\frac{\left(4+\phi^s\right)EI}{L\left(1+\phi^s\right)},\quad K_d=\frac{\left(2-\phi^s\right)EI}{L\left(1+\phi^s\right)}.$$

$$\boldsymbol{G}^e=2\rho AL\begin{bmatrix}
0 & 0 & 0 & 0 & 0 & 0 & 0 & 0 & 0 & 0 & 0 & 0 \\
0 & 0 & G_a & 0 & G_b & 0 & 0 & 0 & -G_a & 0 & G_b & 0 \\
0 & -G_a & 0 & 0 & 0 & G_b & 0 & G_a & 0 & 0 & 0 & G_b \\
0 & 0 & 0 & 0 & 0 & 0 & 0 & 0 & 0 & 0 & 0 & 0 \\
0 & -G_b & 0 & 0 & 0 & G_c & 0 & G_b & 0 & 0 & 0 & G_d \\
0 & 0 & -G_b & 0 & -G_c & 0 & 0 & 0 & G_b & 0 & -G_d & 0 \\
0 & 0 & 0 & 0 & 0 & 0 & 0 & 0 & 0 & 0 & 0 & 0 \\
0 & 0 & -G_a & 0 & -G_b & 0 & 0 & 0 & G_a & 0 & -G_b & 0 \\
0 & G_a & 0 & 0 & 0 & -G_b & 0 & -G_a & 0 & 0 & 0 & -G_b \\
0 & 0 & 0 & 0 & 0 & 0 & 0 & 0 & 0 & 0 & 0 & 0 \\
0 & -G_b & 0 & 0 & 0 & G_d & 0 & G_b & 0 & 0 & 0 & G_c \\
0 & 0 & -G_b & 0 & -G_d & 0 & 0 & 0 & G_b & 0 & -G_c & 0
\end{bmatrix}$$

Where

$$G_a = \frac{6I/5A}{L^2(1+\frac{12EI}{GA^sL^2})^2}, G_b = \frac{-(1/10-1/2\frac{12EI}{GA^sL^2})I/A}{L(1+\frac{12EI}{GA^sL^2})^2},$$

$$G_c = \frac{(2/15+1/6\frac{12EI}{GA^sL^2}+1/3(\frac{12EI}{GA^sL^2})^2)I/A}{(1+\frac{12EI}{GA^sL^2})^2}, G_d = \frac{-(1/30+1/6\frac{12EI}{GA^sL^2}-1/6(\frac{12EI}{GA^sL^2})^2)I/A}{(1+\frac{12EI}{GA^sL^2})^2},$$

and the effective shear area, A^s, is given by: $A^s = A\Big/\frac{7+6\mu}{6(1+\mu)}\left[1+\frac{20+12\mu}{7+6\mu}\left(\frac{Dd}{D^2+d^2}\right)^2\right]$

(3) Rigid disk unit

For the disk, the transmission gear, etc. which could be regarded as rigid disk with rotational effect. They could be simplified as lumped mass units, which makes the lumped mass and the concentrated rotational inertia acting on the corresponding nodes. The number of degrees of freedom is 6, which are the displacement of the three coordinate axes in the local coordinate system and the rotation angle around the axis, as shown in Figure 7.

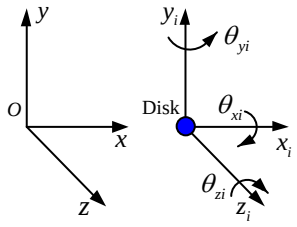

Fig. 7. The schematic diagram of rigid disk unit

The displacement vector of rigid disk unit could be expressed as:

$$\boldsymbol{u} = \begin{bmatrix} x & y & z & \theta_x & \theta_y & \theta_z \end{bmatrix}^{\mathrm{T}}$$

The mass through the axis, rotational inertia of diameter and polar rotational inertia are regarded as m, J_d, and J_p, respectively, then the differential equation of motion of the turntable is:

$$\boldsymbol{M}_d\ddot{u} + \Omega\boldsymbol{G}_d\dot{u} = \boldsymbol{F}_d \tag{4}$$

In equation (4), Ω is the rotational speed of the turntable, $\boldsymbol{F}_d$ is the generalized force vector. $\boldsymbol{M}_d$ and $\boldsymbol{G}_d$ are the mass matrix and the gyro force matrix of the rigid disk unit, respectively, written as:

$$\boldsymbol{M}_d = \begin{bmatrix} m & 0 & 0 & 0 & 0 & 0 \\ 0 & m & 0 & 0 & 0 & 0 \\ 0 & 0 & m & 0 & 0 & 0 \\ 0 & 0 & 0 & J_p & 0 & 0 \\ 0 & 0 & 0 & 0 & J_d & 0 \\ 0 & 0 & 0 & 0 & 0 & J_d \end{bmatrix} \quad \boldsymbol{G}_d = \begin{bmatrix} 0 & 0 & 0 & 0 & 0 & 0 \\ 0 & 0 & 0 & 0 & 0 & 0 \\ 0 & 0 & 0 & 0 & 0 & 0 \\ 0 & 0 & 0 & 0 & 0 & 0 \\ 0 & 0 & 0 & 0 & 0 & -J_p \\ 0 & 0 & 0 & 0 & J_p & 0 \end{bmatrix}$$

ISSN 2572-4975 (Print), 2572-4991 (Online)

(4) Support unit

According to the dynamic principle of the oil-film force of the bearing bush, when the mass of the bearing is neglected, the bearing support can be simplified as a spring-damping unit acting on the support of the rotor in the finite element model of the rotor system. For general pedestal bearings, the coupling force model is shown in Figure 8.

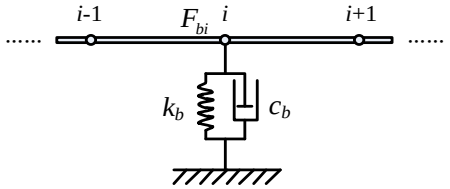

Fig. 8. The schematic diagram of support unit

Assuming that the coupling node between one end of the bearing and the rotor is i and the other end is considered to be fully constrained. The control equation of the bearing is:

$$\boldsymbol{C}_b\dot{\boldsymbol{u}}_i + \boldsymbol{K}_b\boldsymbol{u}_i = \boldsymbol{F}_b \tag{5}$$

In equation (5), $\boldsymbol{u}_i$ is the displacement vector of the support unit, expressed as $[x_i\ y_i\ z_i\ \theta_{xi}\ \theta_{yi}\ \theta_{zi}]^{\mathrm{T}}$, $\boldsymbol{F}_b$ is the generalized force vector, $\boldsymbol{C}_b$ and $\boldsymbol{K}_b$ are the mass matrix and the stiffness matrix of the bearing after bearing force linearization, respectively, written as:

$$\boldsymbol{K}_b = \begin{bmatrix} k_{xx} & 0 & 0 & 0 & 0 & 0 \\ 0 & k_{yy} & k_{yz} & 0 & 0 & 0 \\ 0 & k_{zy} & k_{zz} & 0 & 0 & 0 \\ 0 & 0 & 0 & 0 & 0 & 0 \\ 0 & 0 & 0 & 0 & 0 & 0 \\ 0 & 0 & 0 & 0 & 0 & 0 \end{bmatrix} \quad \boldsymbol{C}_b = \begin{bmatrix} c_{xx} & 0 & 0 & 0 & 0 & 0 \\ 0 & c_{yy} & c_{yz} & 0 & 0 & 0 \\ 0 & c_{zy} & c_{zz} & 0 & 0 & 0 \\ 0 & 0 & 0 & 0 & 0 & 0 \\ 0 & 0 & 0 & 0 & 0 & 0 \\ 0 & 0 & 0 & 0 & 0 & 0 \end{bmatrix}$$

(5) System material damping

The material damping $\boldsymbol{C}_m$ in the system is defined in terms of Rayleigh damping, as follows:

$$\boldsymbol{C}_m = \alpha \cdot \boldsymbol{M}_m + \beta \cdot \boldsymbol{K}_m \tag{6}$$

In equation (6), $\boldsymbol{M}_m$ is the mass matrix of the material, $\boldsymbol{K}_m$ is the stiffness matrix of the material, α, β are the proportional coefficients and can be obtained as:

$$\alpha = 2\left(\frac{\xi_2}{\omega_2} - \frac{\xi_1}{\omega_1}\right) \Big/ \left(\frac{1}{\omega_2^{\,2}} - \frac{1}{\omega_1^{\,2}}\right)$$

$$\beta = 2\left(\xi_2\omega_2 - \xi_1\omega_1\right) \Big/ \left(\omega_2^{\,2} - \omega_1^{\,2}\right)$$

Where ξ_1 and ξ_2 are the damping coefficients, ω_1 and ω_2 are the first two natural frequencies of the system.

(6) Establishing the differential equations of motion of the system

The units mentioned above are used to establish the model of the rotor system comprehensively. Since in the GTF low pressure rotor system, each rotor of the star gear transmission system rotates without revolution. The above-mentioned meshing unit can be applied to the meshing portion of the internal ring gear. Therefore, there are eight

pairs of gear meshing units in the entire rotor system. According to the equations (2) ~ (6), FEM model of low pressure rotor can be set up by grouping the mass matrix, stiffness matrix, damping matrix, etc. And the schematic diagram of the superposition of the stiffness matrix is shown in Figure 9.

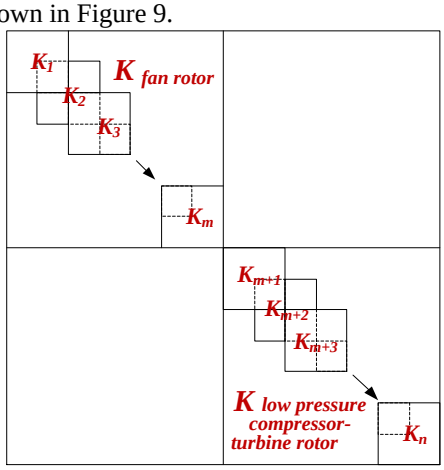

Fig. 9. The schematic diagram of the superposition of the stiffness matrix

The differential equation of motion of the entire rotor system is:

$$\boldsymbol{M}\ddot{\boldsymbol{X}} + (\boldsymbol{C} + \boldsymbol{\Omega G})\dot{\boldsymbol{X}} + \boldsymbol{K}\boldsymbol{X} = \boldsymbol{F}$$

Where, $\boldsymbol{M}$ is the mass matrix of the system, $\boldsymbol{C}$ is the damping matrix of the system, including bearing damping, material damping, etc. $\boldsymbol{G}$ is the gyro matrix of the system, $\boldsymbol{\Omega}$ is the rotational speed of the rotor, $\boldsymbol{K}$ is the stiffness matrix of the system, and $\boldsymbol{F}$ is the generalized force vector subjecting to the system, including unbalanced force vectors, external additive loads, etc. $\boldsymbol{X}$ is the displacement vector for each node and is expressed as:

$$\boldsymbol{X} = [u_1, v_1, w_1, \theta_{x1}, \theta_{y1}, \theta_{z1}, u_2, v_2, w_2, \theta_{x2}, \theta_{y2}, \theta_{z2}, \cdots, u_n, v_n, w_n, \theta_{xn}, \theta_{yn}, \theta_{zn}]^{\mathrm{T}}$$

3 Inherent characteristic analysis and model verification of low pressure rotor system

In this chapter, the influence of gear coupling on the dynamic characteristics of a low pressure rotor system with star shaped gears will be analyzed. The modes of rotor system with and without considering the coupling effect of gear will be calculated by MATLAB. At the same time, the results are compared with the simulation results of Samcef Field to verify the model.

3.1 Simulation model of rotor system based on Samcef Field

Considering the low pressure rotor system with star shaped gears drive structure as the study object, the mixed modelings with one-dimensional beam element and three-

ISSN 2572-4975 (Print), 2572-4991 (Online)

dimensional solid element are established as shown in Figure 10. This model is used to verify the reliability of the finite element numerical model considering coupling effect of gear.

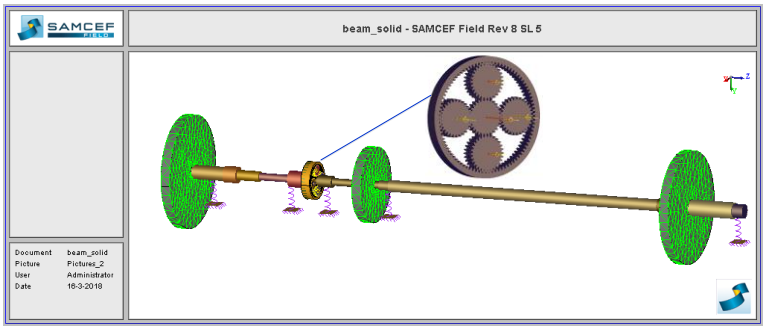

Fig. 10. Rotor model build on Samcef Field

The material density of the rotor model is 7850kg/m^3, and modulus of elasticity is 209Gpa. The disc is divided into grid by tetrahedral element, and the rotor system consists of 5587 elements and 9597 nodes. Rotor supports are simulated by rotor spring elements. The connection between the fan rotor and the low pressure compressor-turbine rotor is defined by special gear assembly unit in Samcef Field engineering software. In this study, the influence of the gear deformation on the coupled vibration of the fan rotor and the compressor turbine rotor is ignored, so the gears are considered as rigid body.

3.2 The influence of gear coupling on the inherent characteristics of the rotor system

Under the same supportings and structural parameters, analysis results based on MATLAB and Samcef Field are shown in Table 2 respectively. The multi order modes of fan rotor combined with low pressure compressor-turbine rotor are analyzed. When considering the coupling effect of gear, the inherent characteristics of low pressure rotor system will change. The first 10 modes of the rotor system consists the first 2 modes of the fan rotor and the first 7 order modes of the low pressure compressor turbine rotor. The corresponding modal shapes are shown in figures 11 and 12, respectively. Table 3 lists the two natural frequencies of the single rotor and the first 10 order natural frequencies of a low pressure rotor system considering the coupling effect of gear.

Table 2. The first 10 order modes of low pressure rotors

Order	MATLAB simulation	Samcef Field simulation

1	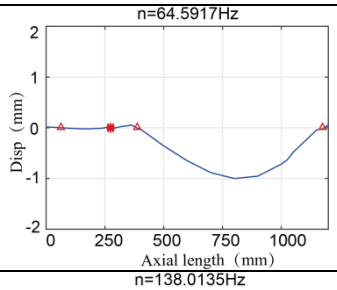	
2	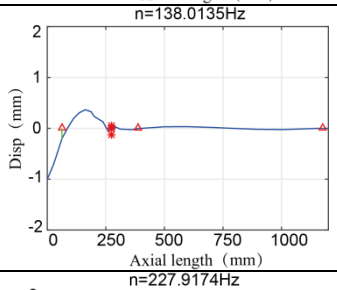	
3	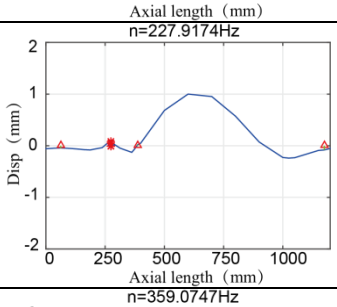	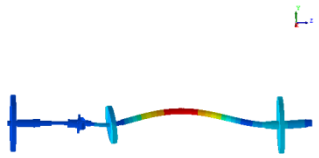
4	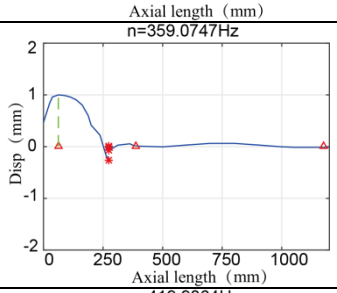	
5	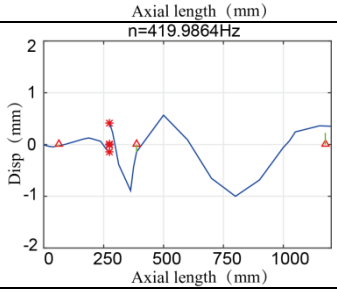	

ISSN 2572-4975 (Print), 2572-4991 (Online)

6	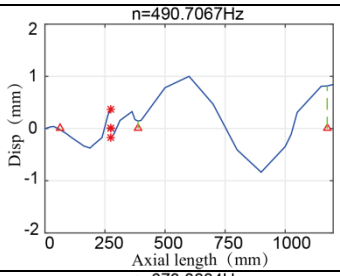 n=490.7067Hz Disp (mm) Axial length (mm)	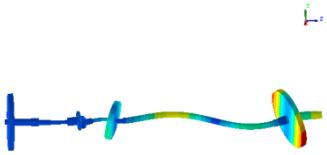
7	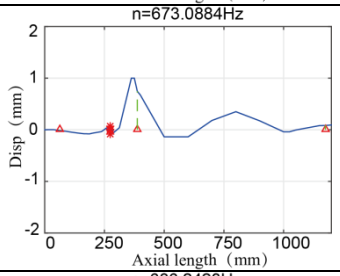 n=673.0884Hz Disp (mm) Axial length (mm)	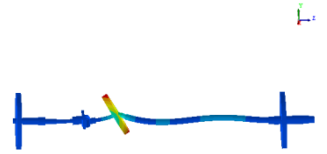
8	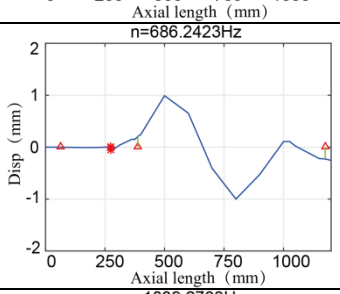 n=686.2423Hz Disp (mm) Axial length (mm)	
9	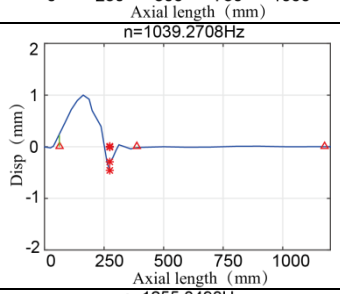 n=1039.2708Hz Disp (mm) Axial length (mm)	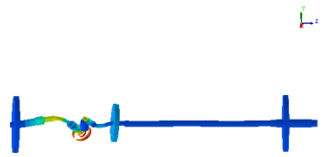
10	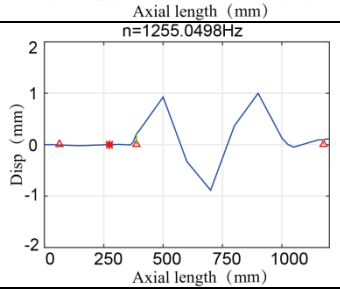 n=1255.0498Hz Disp (mm) Axial length (mm)	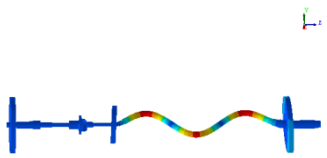

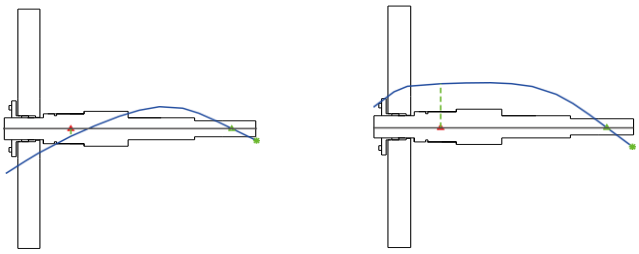

(a) 1st order (b) 2nd order

Fig. 11. The first 2 order modes of fan rotor

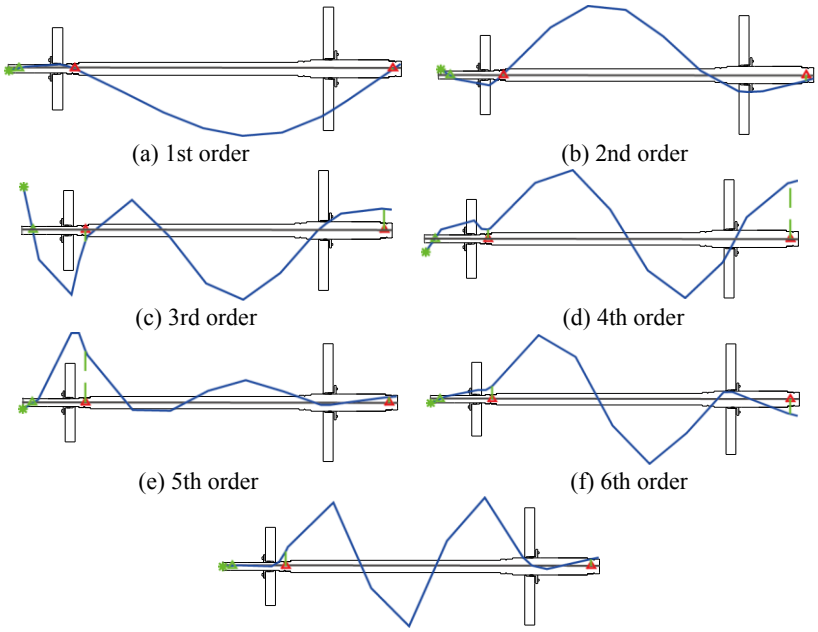

(a) 1st order (b) 2nd order

(c) 3rd order (d) 4th order

(e) 5th order (f) 6th order

(g) 7th order

Fig. 12. The first 7 order modes of low pressure compressor-turbine rotor

Table 3. Natural frequencies of rotors (Hz)

Order	Single rotor	Low pressure rotor	Source of natural frequencies
1	64	64	Low pressure compressor-turbine rotor
2	128	138	Fan rotor
3	225	228	Low pressure compressor-turbine rotor
4	354	359	Fan rotor
5	403	420	Low pressure compressor-turbine rotor
6	489	491	Low pressure compressor-turbine rotor
7	673	673	Low pressure compressor-turbine rotor
8	686	686	Low pressure compressor-turbine rotor
9	--	1039	Coupling derivative

ISSN 2572-4975 (Print), 2572-4991 (Online)

10	1255	1255	Low pressure compressor-turbine rotor

According to the analysis of the above chart, the natural frequencies of the low pressure rotors are partly derived from the fan rotor and the low pressure compressor-turbine rotor. however the values are different due to the new constraints imposed on the two rotors respectively which comes from the gear engagement. In addition, compared to the low pressure rotors, the calculation of a single rotor model has lost some inherent frequency, such as the 9th order coupling derivative frequency in Table 2. Therefore, in the study of the dynamic characteristics of the low pressure rotor system of GTF engine, the coupling effect of the gear must be considered in order to prevent missing important information.

It can be seen from the system vibration mode drawing based on MATLAB, for coupled vibration of the whole machine system, most of the prototype can be found from the single rotor vibration frequency. The 9th order is a complex mode of vibration corresponding to the derived frequency. It can be found from the analysis of natural frequencies and vibration modes that the complex vibration modes of the system are formed due to the coupling of the single rotor vibration modes at the corresponding frequency and the vibration of the other rotor. It can be seen that the vibration of a single rotor in the system can stimulate the vibration of other rotors to form a complex vibration mode through the mesh of the gear. It shows that two rotors are no longer independent systems after the gear coupling and its dynamic characteristics will interact with each other. In addition, for the other four gear rotors with the exception of the fan rotor and the low pressure compressor-turbine rotor, because of the small quality, the short rotating shaft and the large support stiffness, its individual action is not obvious in the coupling action of each rotor. Therefore, the vibration modes of the whole system are mainly composed of the fan rotor and the low pressure compressor-turbine rotor.

According to table 2, through comparing the system vibration modes based on MATLAB and the system vibration modes based on Samcef Field, it can be seen that most of the results are consistent. Comparison of the calculated natural frequencies of the low pressure rotor system is shown in table 4.

Table 4. Comparison of natural frequencies calculated by MATLAB and Samcef Field

Order	MATLAB simulation result	Samcef Field simulation result	error
1	64	63	1.6%
2	138	143	3.6%
3	228	225	1.3%
4	359	346	3.6%
5	420	388	7.6%
6	491	462	5.9%
7	673	633	5.9%
8	686	666	2.9%
9	1039	934	10.1%
10	1255	1217	3.0%

It can be seen from Table 4, among the calculation results of the natural frequency of the rotor system based on MATLAB, except for the ninth order, the errors of the rest

are less than 10% compared with the inherent frequency calculation results based on Samcef Field. The reliability of numerical analysis method and the simulation model can be verified within the allowable range of error. The difference of the ninth order coupling derivation frequency is mainly caused by the difference between the two modeling methods for the processing of the gear meshing part of the system. In addition, the calculation errors of the natural frequency of the 2nd, 4th, 5th, 6th, and 7th order are relatively larger. It can be seen from the corresponding mode graph, the maximum deformation of the rotor system at these frequencies are on the disks, so it is known that the calculation error mainly derives from the model simplification in the numerical analysis and calculation. The discs are all simplified as a rigid disc element, and the vibration effect of the disc is ignored.

3.3 Vibration mode test

Figure 13 shows a experiment rig of GTF low pressure rotor system which was built based on structural similarity and equal-proportion principle. The natural frequencies of the rotor system are measuring with hammering methods. Both the fan rotor and the low pressure compressor turbine rotor have a measuring point respectively. According to the sampled vibration time domain signal, the results obtained are shown in Figure 14 through Fourier transform.

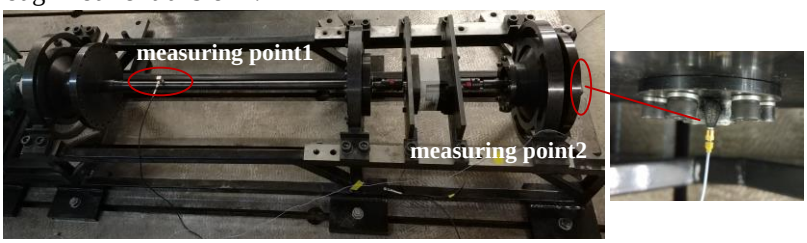

Fig. 13. Experiment rig of GTF low pressure rotor system

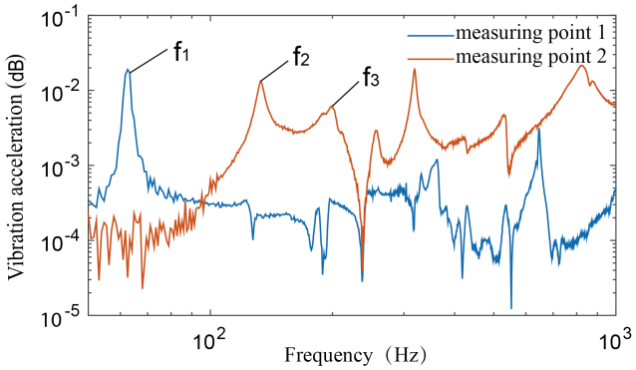

Fig. 14. Natural frequencies of rotor system

ISSN 2572-4975 (Print), 2572-4991 (Online)

According to the test results, comparing the first three natural frequencies of the rotor system with the results calculated by MATLAB, the errors of the first two orders are both less than 10%, the correctness of the theoretical modeling method is further confirmed. The error of the third order in Table 5 is large, in addition, the test results also have other frequencies that have a larger error with the simulation results, mainly due to the installation error and the influence of multiple parts in the experiment rig.

Table 5. Comparison of natural frequencies based on MATLAB and Test

Order	Test result	Simulation result	Error
1	62.5	64	2.3%
2	132	138	4.3%
3	200.8	227	11.5%

4 Coupled vibration analysis of low pressure rotor system

4.1 Unbalance response analysis

The unbalance excitation is applied to the rotor system fan disk, low pressure compressor disk and low pressure turbine disk of a low pressure rotor system finite element model with star shaped gear drive structure established by MATLAB. The working condition parameters is shown in Table 6. The vibration response of fan rotor support Lp-1#, low pressure compressor-turbo rotor support Lp-2#, Lp-3# and gearbox support G-1 and G-2 are analyzed with and without consideration of the gear coupling effect by precise integration method.

Table 6. Working condition of rotor system

Unbalanced position	Node number	Amount of unbalance (g·mm)	Initial phase (deg)
Fan disk	2	4000	0
Low pressure compressor disk	19	6000	0
Low pressure turbine disk	30	4000	0

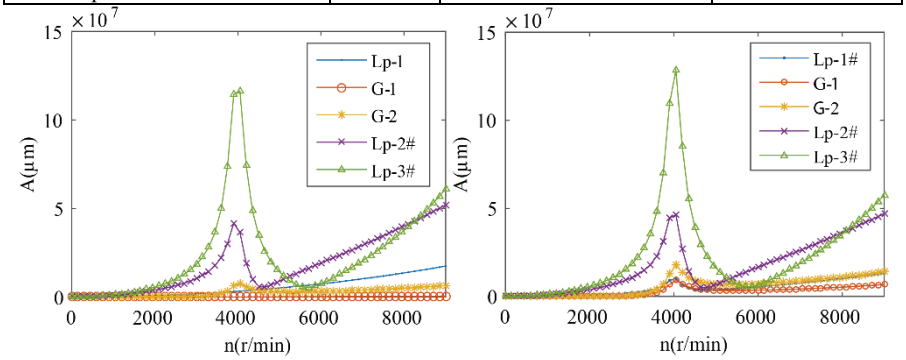

(a) without consideration of the gear coupling effect

(b) with consideration of the gear coupling effect

Fig. 15. Amplitude frequency response of the rotor supports

The amplitude frequency response curves of the rotor supports are described in Figure 15 when there is amount of unbalance on the fan rotor and the low pressure compressor-turbine rotor. As shown in Fig.15b, there is a peak of vibration at all pivot points when the input shaft speed is in the range of 3900r/min-4050 r/min, which is corresponding to the first critical speed 3840r/min of rotor system. Compared with the Fig.15a, there is a peak frequency of the supports Lp-1# and G-1 because of the gear coupling effect, and the peak frequency of the amplitude frequency response curve of the supports G-2 and Lp-3# is more obvious.

The working condition parameters of rotor system shown in Table 6 are divided into two parts: imbalance of fan disk, imbalance of low pressure compressor disk and low pressure turbine disk. Considering the gear coupling effect, unbalance response of the rotor system is analyzed at the gearbox supports G-1 and G-2 under three working conditions of 1800r/min, 2100 r/min and 2400 r/min. The gear meshing frequency is high and the acceleration signal can reflect the high-frequency components accurately compared to the displacement signal, therefore, only the vibration acceleration signal is extracted and analyzed from the study of coupling vibration.

Table 7. Vibration characteristics of two supports of gearbox under different working conditions (1800 r/min)

Imbalance location	Support G-1	Support G-2
Fan disk	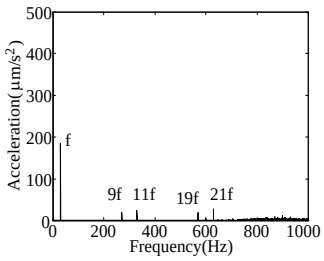	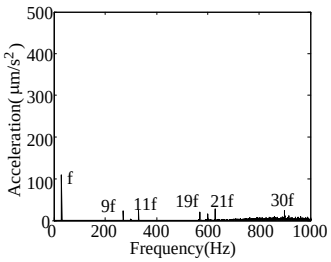
Low pressure compressor disk and low pressure turbine disk	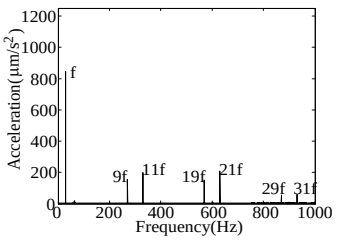	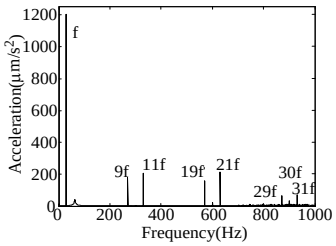

 ISSN 2572-4975 (Print), 2572-4991 (Online)

All disks	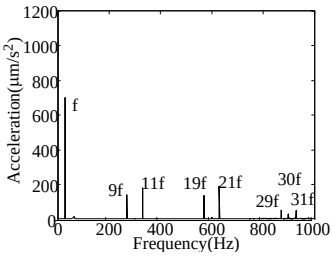	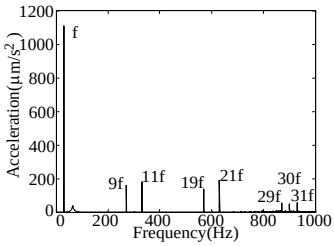

Table 8. Vibration characteristics of two supports of gearbox under different working conditions (2100 r/min)

Imbalance location	Support G-1	Support G-2
Fan disk	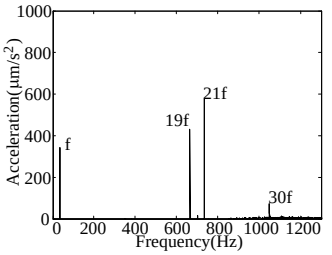	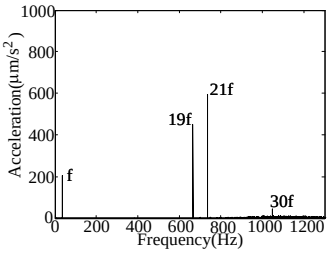
Low pressure compressor disk and low pressure turbine disk	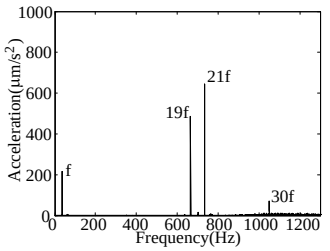	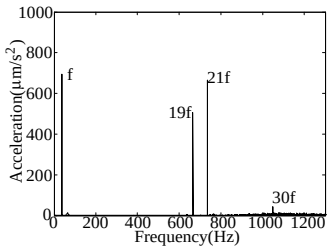
All disks	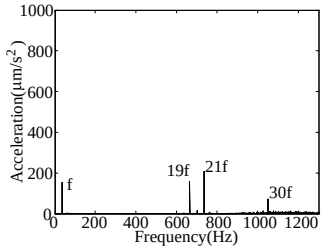	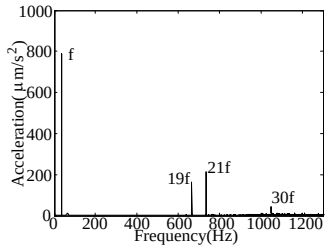

Table 9. Vibration characteristics of two supports of gearbox under different working conditions (2400r/min)

Imbalance location	Support G-1	Support G-2

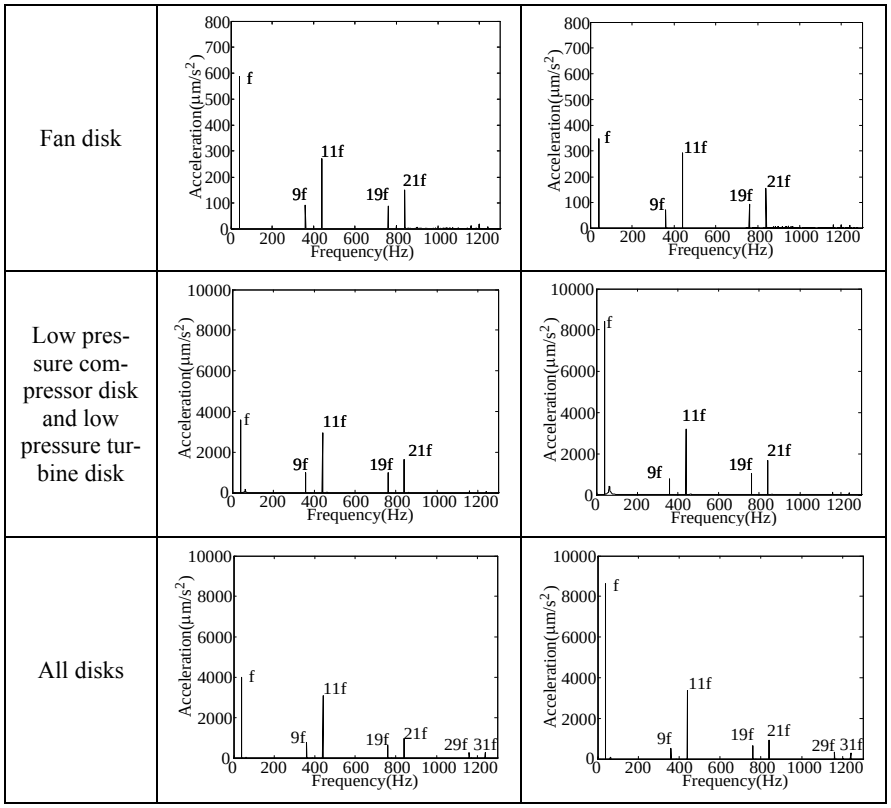

Because of the gear coupling effect, the vibration caused by the unbalance of the single rotor is transmitted to the other axis through the gear meshing, which causes the vibration of the whole rotor system. From table 7~9, there are multiple frequency components in the rotor system with rotational frequency. The proportion of each frequency is different under different speeds, and the more imbalances exist in the rotor system, the more complex the frequency domain components are. In the response spectrum, f represents the rotational frequency of the input axis, and the 30f is the meshing frequency of the rotor system.

According to transverse analysis of table 7~9, when there is only imbalance of fan disk in the rotor system, vibration acceleration of each support increases with increase of speed shown in the spectrum diagram of two gearbox supports at different speeds. The vibration acceleration of the support G-1 is slightly greater than that of the support G-2 at different rotational speeds, and the vibration acceleration difference between the two supports increases with the increase of the speed. Due to the imbalance of the low pressure compressor-turbine rotor, it can be seen from table that the difference between the two supports' vibration acceleration is still increasing with the increase of speed. However, the vibration of the support G-2 become stronger than G-1, and both vibration no longer keep increasing. Taking the support G-1 as an example, when the rotor speed is 1800 r/min, the vibration acceleration value reaches 800 μm/s^2, and when the rotor speed increases to 2100 r/min, the vibration acceleration of the support is less than 300

 ISSN 2572-4975 (Print), 2572-4991 (Online)

μm/s^2, which is mainly caused by the interaction of imbalance low pressure compressor disk and low pressure turbine disk.

The vibration response of the gearbox supports with imbalance of three disks in the rotor system is analyzed. It can be clearly seen from table that under all three speeds, the vibration acceleration values of the supports are approximately the same as those of the rotor system with imbalance of low pressure compressor disk and low pressure turbine disk. As a result, compared with the fan rotor, the imbalance of the low pressure compressor-turbine rotor has a greater impact on the vibration characteristics of the rotor system. In addition, taking the vibration of the support G-1 in table 8 shows as an example, when the speed is 2100 r/min, the vibration acceleration in G-1 is minimum with imbalance of three disks, which shows that if there is an imbalance in the rotor system, gear vibration and impact can be reduced through adding the weight in the other parts of the system.

4.2 Test of imbalanced rotor

The rotor test is carried out for the three working conditions of imbalance of fan disk, low pressure compressor disk and low pressure turbine disk and all disks. To exclude the interference waveform caused by static electricity and other factors and identify the meshing frequency, the speed frequency is set to 31Hz. Gearbox is selected to arrange the sensor and vibration acceleration parameter synthesis test method is used to get the vibration signal. The time domain waveform and spectrum of the vibration response at the gearbox are shown in Figure 16.

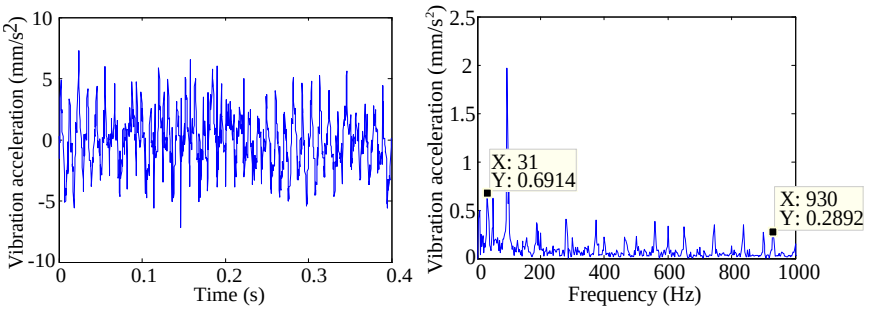

(a) Imbalance of fan disk

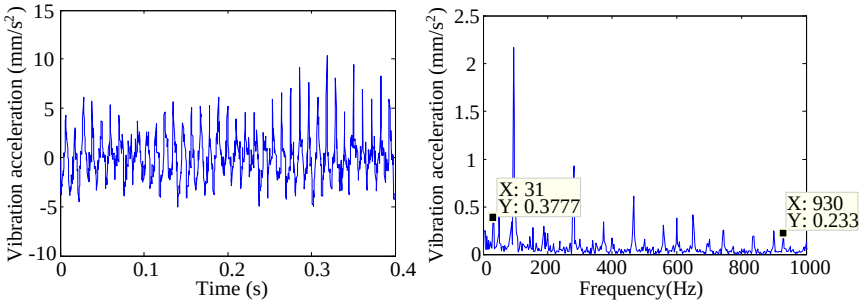

(b) Imbalance of low pressure compressor disk and low pressure turbine disk

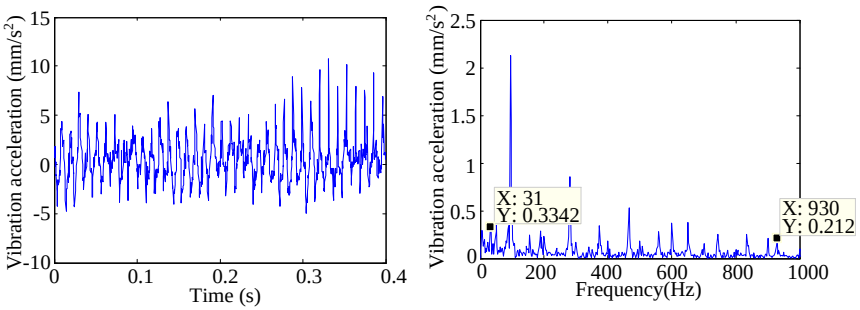

(c) Imbalance of all disks

Fig. 16. Vibration response of rotor system under different working conditions

As shown in the time domain waveform, the vibration characteristics at the gearbox of rotor system with imbalance of three disks tend to be consistent with that of rotor system with imbalance of low pressure compressor disk and low pressure turbine disk and the frequency components of the rotation are also similar. Moreover, vibration peak of the rotational frequency is the smallest under the condition of imbalance of three disks compared with that under the three conditions. It is further explained that the imbalance of low pressure compressor disk and low pressure turbine disk has an important influence on the vibration in the gear rotor system and the gear vibration and impact can be reduced through adding the weight in the other parts of the system. In addition, 930Hz is detected in all three working conditions, and it is 30 times of the rotational frequency, which is the meshing frequency of the gear. There are some other frequency components in frequency domain diagram apart from frequency doubling of rotational frequency, which mainly come from the influence of natural frequency of some parts in rotor system.

5 Conclusions

Aiming at GTF low pressure rotor system, a three-support rotor with star gear transmission system was built. Through the dynamic analysis and calculation of the rotor system, the following conclusions are obtained.

(1) Through simulation and experimental comparison, it is shown that the meshing part of gears in the rotor system is simplified to the spring damping element, which can simulate the coupling action of gears well and establish a precise coupling integral model.

(2) The calculation of the fan and the low pressure compressor-turbine rotor in the low pressure rotor system will make the natural frequency offset and the partial mode loss, resulting in unreliable calculation results. Therefore, the coupling action of gears must be considered in the study of the dynamic characteristics of the GTF engine rotors, so as to prevent missing important information.

(3) Considering the coupling action of gears, the unbalance response of the rotor system under different operating conditions shows that, compared with the fan rotor,

 ISSN 2572-4975 (Print), 2572-4991 (Online)

the imbalance of the low pressure compressor-turbine rotor has a greater influence on the vibration characteristics. In addition, the position of unbalance will change the variation of rotor's vibration with rotational speed. In the spectrum analysis, because of the coupling of gears, the rotor system has multiple frequency components of rotational frequency, and the ratio of each frequency is different at different speed.

(4) Through the simulation, the vibration signal of the gearbox in the rotor system at constant speed is collected, and the coupling vibration of the rotors is verified. It is further explained that if the unbalance of rotor system causes the impact vibration of gears, the effect of vibration can be reduced by the other parts. This problem belongs to the field of dynamic balance, and it needs to be further studied according to relevant theories.

Acknowledgement

This work is supported by the National Natural Science Foundation of China (No.51705064).

References

1. D.Z. Zhang, J.X. Zhang, F. Wang, Analysis of Structual Design Characteristics for Geared Turbofan Engine, ***Aerogine***, 37 (2011) 1-4.
2. J. Li, Overview of Advanced Technology for Geared Turbofan Engine, ***Aerogine***, 35 (2009) 55-58.
3. Z.D. Fang, Y.W. Shen, Z.D. Huang, The Dynamic Behavior of Star Gearing with Three Branches, ***Journal of Aeronautics***, 11(1990) 341-350.
4. Z.M. Sun, Y.W. Shen, S.M. Wang, et al, Nonlinear Dynamic Modeling and Dynamic Tooth Loads Analysis of Star Gearing System, ***Journal of Aeronautics***,16(2001) 402-408.
5. Z.B. Zhu, R.P. Zhu, H.Y. Bao, Nonlinear Dynamic Study of 2-Stage Star Gear Train, ***Journal of Aerospace Power***, 22 (2007) 1963-1970.
6. W.Z. Yan, X. Liao, C. Cao, Structure and dynamic analysis of low pressure rotor in geared turbofan. ***Journal of Aerospace Power***, 30 (12) (2015)2863-2869.
7. Y.H. Ma, C. Cao, Y. Hao, et al., Structure and dynamic analysis of rotor system in geared turbofan engine, ***Journal of Aerospace Power***, 30 (2015) 2753-2761.
8. Z.D. Xu, L.W. Ma, ***Dynamics of Structures***. Beijing: Science Press, 2007.
9. G. Chen, Design Features of PW1000G GTF Engine, ***International Aviation***, 12 (2009) 71-74.
10. J. Feng, K. Qin, D. Wang, Discussion on Conceptual Design of Fan Driver Gear System with Star Gears, ***Advances in Aeronautical Science and Engineering***, 6 (2015) 490-494.
11. M.X. Hou, J.H. Li, M.Q. Zhang, et al., Research on Design Technology of Planetary Gear System for Geared Turbofan Engine, ***Aerogine*** , 40 (2014) 61-64.
12. J.S. Rao, T.N. Shiau, J.R. Chang, Theoretical analysis of lateral response due to torsional excitation of geared rotors, ***Mechanism and Machine Theory***, 33 (1998) 761-783.
13. N. Hagiwara, M. Ida, K. Kikuchi, ***Forced Vibration of a Pinion-Gear System Supported on Journal Bearings***. Transactions of the Japan Society of Mechanical Engineers, 49(1983)1530-1537.

14. R.J. Iannuzzelli, R.M. Elward, Torsional/Lateral Coupling in Geared Rotors, ***International Journal of Turbo and Jet Engines***, 2 (1985)11-18.
15. Zuetbes, Stability behavior of geared rotor systems regarding torsional lateral coupling, ***Rotating Machinery Dynamics***, 18 (1989) 217-224.
16. T. Kiekbusch, D. Sappok, B. Sauer, et al., Calculation of the Combined Torsional Mesh Stiffness of Spur Gears with Two- and Three-Dimensional Parametrical FE Models, ***Strojniski Vestnik***, 57 (2011) 810-818.
17. Z.F. Zhang, H. Zhang, T. Xu, et al., Analysis of Coupling Vibration Characteristics of the Rotor System for Integrally Geared Centrifugal Compressors, ***Noise and Vibration Control***, 35 (2015) 41-46.

 ISSN 2572-4975 (Print), 2572-4991 (Online)